2011 *Plasma Phys. Control. Fusion* 53 **065011 doi:** 10.1088/0741-3335/53/6/065011

Magnetic perturbation experiments on MAST L and H-mode plasmas using internal coils

A. Kirk, Yueqiang Liu, E. Nardon[2], P. Tamain[2], P. Cahyna[3], I. Chapman, P. Denner[4], H. Meyer, S. Mordijck[5], D. Temple[6] and the MAST team

EURATOM/CCFE Fusion Association, Culham Science Centre, Abingdon, Oxon OX14 3DB, UK
[2]Association Euratom/CEA, CEA Cadarache, F-13108, St. Paul-lez-Durance, France
[3]Institute of Plasma Physics AS CR v.v.i., Association EURATOM/IPP.CR, Prague, Czech Republic
[4]University of York, Heslington, York YO10 5DD UK
[5]University of California-San Diego, 9500 Gilman Dr, La Jolla, California 92093, USA
[6]Imperial College of Science, Technology and Medicine, London, UK

Abstract

Experiments have been performed on MAST using internal (n=3) resonant magnetic perturbation coils. The application of the RMPs to L-mode discharges has shown a clear density pump out when the field line pitch angle at the low field side of the plasma is sufficiently well aligned with the applied field. The application of the RMPs before the L-H transition increases the power required to achieve H-mode by at least 30 %. In type I ELM-ing H-mode discharges, at a particular value of q_{95}, the ELM frequency can be increased by a factor of 5 by the application of the RMPs. This effect on the ELMs and the L-mode density pump out is not correlated with the width of the region for which the Chirikov parameter, calculated using the vacuum field, is greater than 1 but may be correlated with the size of the resonant component of the applied field in the pedestal region or with the location of the peak plasma displacement when the plasma response is taken into account.

1. Introduction

In order to avoid damage to in-vessel components in future devices, such as ITER, a mechanism to ameliorate the size of ELMs is required [1]. One such amelioration mechanism relies on perturbing the magnetic field in the edge plasma region, enhancing the transport of particles or energy and keeping the edge pressure gradient below the critical value that would trigger an ELM, while still maintaining an edge transport barrier. This technique of Resonant Magnetic Perturbations (RMPs) has been employed on DIII-D [2], where complete ELM suppression has been possible, and on JET where ELM mitigation has been obtained [3]. A set of in-vessel ELM control coils consisting of two rows of six coils each, one above and one below the mid-plane, similar to the DIII-D I-coils, have been installed in MAST [4]. This paper presents results from the application of RMPs from an n=3 configuration of these coils on MAST L and H-mode Connected Double Null (CDN) and Single Null Divertor (SND) discharges. The results will be compared with modelling in the vacuum field approximation and where the plasma response has been taken into account in order to try to determine which parameters are correlated with the RMPs having an effect on the plasma.

2. Effect of n=3 RMPs on L-mode plasmas

Initial experiments on Ohmic CDN L-mode plasmas, with a plasma current I_P=400kA and q_{95}=6.0, showed a clear density pump out due to the application of the RMPs (with a drop in density (n_e) of up to 35%), together with an increase in the turbulent fluctuation level [4]. For this type of discharge the effect was only observed when the coils were in an even configuration (where the currents in the upper and lower coil at the same toroidal location have the same sign), and not in an odd configuration (the currents in the upper and lower

coil have opposite sign). Calculations of the magnetic perturbation to the plasma due to the coils have been performed using the ERGOS code (vacuum magnetic modelling) [5]. The Chirikov parameter ($\sigma_{Chirikov}$), which is a measure of the island overlap, is used to define the stochastic layer as the region for which $\sigma_{Chirikov}$ is greater than 1 [5]. These calculations show that for this discharge type, the even configuration is much more resonant than the odd one (with radial resonant perturbations larger by a factor >3). In fact as will be discussed below, a density pump out can be produced in either even or odd parity if the coil perturbation is well aligned with the field in the plasma.

Figure 1a and b show the effect of applying the RMPs in Even and Odd parity configurations for a shot which has a plasma current (I_P) of a) 400 kA and b) 900 kA. In the shot with Ip=400 (900) kA an even (odd) parity configuration of the coils produces a density pump out while the odd (even) parity configuration has no effect. This difference suggests that an alignment of the perturbation with the plasma is required. In both cases the toroidal field on axis (B_T) of 0.585 T, however, in spite of the difference in plasma current the value of q_{95} in both cases is ~ 6. This is possible, since on an ST the value of q is dominated by the field at the High Field Side (HFS) of the plasma, which depends on the distance between the HFS plasma edge and the centre column. The shot with the larger I_P is closest to the centre column (see Figure 2a), which results in the same value of q_{95} in the two shots. Figure 2b and c show how the field line pitch angle at the Low Field Side (LFS) is well aligned with the perturbation from the coils in even parity for the plasma with I_P = 400 kA and in odd parity for the plasma with I_P=900 kA respectively. Note that this alignment is expected to remain approximately the same across the plasma edge region.

Since both shots have the same q_{95} this demonstrates that it is not simply the q_{95} which is important but that the alignment of the low field side field lines is a more relevant parameter.

Figure 3 a and b show another way of looking at this alignment, which is to consider the poloidal magnetic spectra of the applied perturbation (b^1) as a function of poloidal mode number (m) and normalised radius ($\Psi_{pol}^{1/2}$). b^1 represents the normalised component of the perturbed field perpendicular to equilibrium flux surfaces and is given by $b^1 \equiv \left(\vec{B} \cdot \vec{\nabla} \psi_{pol}^{1/2} \right) \Big/ \left(\vec{B} \cdot \vec{\nabla} \varphi \right)$ where $\vec{B}$ is the total field vector and φ is the toroidal angle [6]. Superimposed on the spectra are the locations of the q=m/3 rational surfaces. The applied perturbation is resonant (i.e. the rational surface locations are well aligned with the peaks in the applied perturbation) in the even parity configuration for the plasma with I_p=400 kA and in the odd parity configuration for the plasma with I_p = 900 kA.

The effective radial resonant field component of the n=3 applied perturbation normalised to the toroidal field (b^r_{res}) is the amplitude of the resonant Fourier component in the spectrum of b^1 divided by the average value of $\vec{\nabla} \psi_{pol}^{1/2}$ on the magnetic surface, normalized to the major radius (see page 47 of reference [6]): $b^r_{res} = 2 \left| b^1_{m=qn,n} \right| \Big/ R_0 \left\langle \vec{\nabla} \psi_{pol}^{1/2} \right\rangle$. The radial profile of b^r_{res} for both discharges is shown in Figure 4a. Although the profiles have a slightly different shape the maximum value of ~ 5×10^{-4} is similar for both discharges where the density pump out is observed. The RMP spectrum is dominated by the n=3 harmonic and so other harmonics are neglected. Resonant surfaces are characterized by q=m/3 and the Chirikov parameter is calculated in-between each pair of resonant surfaces

as: $\sigma_{Chirikov} = (\delta_m + \delta_{m+1})/\Delta_{m,m+1}$, where δ_m and δ_{m+1} represent the half-widths of the magnetic islands on the q=m/n and q=(m+1)/n surfaces (m being the poloidal mode number and q the safety factor) and $\Delta_{m,m+1}$ the distance between these two surfaces. The Chirikov parameter profiles for both shots are shown in Figure 4b. Again the profiles are similar and the region for which the Chirikov parameter is greater than 1 ($\Delta_{\sigma Chirikov>1}$) is 0.11 in units of $\sqrt{\psi_{pol}}$ or ~ 0.2 in units of ψ_{pol}.

To try to determine if it is the size of the b^r_{res}, $\Delta_{\sigma Chirikov>1}$ or another parameter that is most important in determining whether or not a pump out is observed, a shot has been established which is not perfectly aligned with the coils in either even or odd parity. This shot has I_p=750 kA and pump out is only observed when the coils are in an even parity configuration (see Figure 5 a and b). The Chirikov parameter profile for both configurations is similar (see Figure 5c), with both predicted to have a large region for which $\sigma_{Chirikov}>1$, with $\Delta_{\sigma Chirikov>1}$=0.165 in units of ψ_{pol} in both cases. The maximum value of the normalised resonant component of the applied field (b^r_{res}) is slightly larger in the case of even parity where pump out is observed ($b^r_{res}=4.7\times10^{-4}$) than in odd parity ($b^r_{res} = 3.7\times10^{-4}$) (see Figure 5d). In order to see how other non-axisymmetric fields affect these calculations, the n=3 components of the intrinsic error fields and the error field correction coils on MAST have been added to those produced by the ELM coils and included into the ERGOS modelling. The Chirikov parameter profile is little altered by the addition of these fields (Figure 5c) but the small difference in the initial b^r_{res} profile is slightly increased (see Figure 5d). However, this change is insignificant compared to the change that occurs when the plasma response is considered.

Calculations have been performed using the MARS-F code, which is a linear single fluid resistive MHD code that combines the plasma response with the vacuum perturbations, including screening effects due to toroidal rotation [7]. These calculations show an amplification of the non-resonant (m<0) components (i.e. the modes that have opposite helicity to the field lines) but a significant reduction in the resonant components due to screening effects. The calculations use the experimental profiles of density, temperature and toroidal rotation as input and realistic values of resistivity, characterised by the Lundquist number (S) which varies from ~10^8 in the core to ~10^6 in the pedestal region (the radial profile of the resistivity is assumed proportional to $T_e^{-3/2}$).

The resistive plasma response significantly reduces the field amplitude near rational surfaces and reduces the resonant component of the field by more than an order of magnitude (Figure 5d) with the reduction being largest in the case of odd parity. The Chirikov parameter profile is also reduced (Figure 5c) and the Chirikov parameter only just exceeds 1 at the edge of the profile and only in the case of even parity. In the MARS-F modelling the RMP field also causes a 3D distortion of the plasma surface, which potentially leads to the formation of a 3D steady state equilibrium. Figure 6a shows the normal displacement of the plasma surface as a function of poloidal angle. For the case of odd parity, the displacement is peaked near the mid-plane (θ=0°), while for even parity the displacement is peaked near the X-points (represented by the dashed vertical lines). The maximum displacement is of the order of several mm/kAt i.e. for the coil current used (5.6kAt) the maximum displacement is ~ 16mm.

Similar calculations have been performed for the shots with I_P=400 kA (Figure 6b) described above where a density pump out was observed in even parity. Again for the coil

configuration where the pump out is observed the ratio of the displacement at the poloidal location near to the X-point to that at the mid-plane is greater than 1. The location of the peaking of the displacement at the X-point is not just correlated with the configuration of the coils as can be demonstrated by considering the shot with I_p= 900 kA (Figure 6c) described above where the density pump out is only observed in odd parity. Although the largest predicted displacement is in even parity this is located at the mid-plane. However, in odd parity where the pump out is observed, the surface displacement is predicted to peak at the X-point. In fact in all the shots observed to date, density pump-out only occurs when the predicted surface plasma displacement is larger at the X-point than at the mid-plane [8]. One reason that the location of the displacement may be important could be related to the fact that the X-point is normally considered to be the dominant fuelling location, from recycling, for the plasma. Hence modifications to this region of the plasma may change the relationship between sources and sinks in the overall particle balance equation and lead to a reduction of the density. A study using MARS-F of the poloidal harmonics triggered by the application of the RMPs shows that the peaking of the displacement near the X-point is correlated with the excitation of a stable peeling-like mode near to the plasma edge [9] and this too may have an effect on the density evolution.

The plasma response modelling shows the importance of screening due to plasma rotation. In order to investigate this the shot with I_p=400 kA has been repeated with and without RMP with the addition of neutral beam heating to apply a torque to the plasma while still keeping the plasma in L mode. The size of the pump out observed in these beam heated shots (see Figure 7a) is similar to that observed in shots at the same density without neutral beam injection. The injection of 2 MW of beam power not only heats the plasma

but increases the toroidal rotation near to the plasma edge (ψ_{pol}=0.95 which is at R=1.32 m) from 7 kms^{-1} to 25 kms^{-1} (see Figure 7b). This suggests that there is little evidence that this change in toroidal rotation, on its own, affects the screening of the RMPs by the plasma. MARS-F has been used to model the change in screening and plasma response due to this change in plasma rotation. Figure 8a and b show the profiles of b^r_{res} and $\sigma_{Chirikov}$ which are very similar for the two cases. Although a large screening occurs when going from the vacuum (max $b^r_{res}=5x10^{-4}$) to the plasma response calculation (max $b^r_{res}=1.4x10^{-4}$) subsequent small changes in the rotation profiles do not have a large effect on the resonant components. In order to modify the profiles significantly, more than an order of magnitude reduction in rotation, especially near to the plasma edge is required [8].

3. Effect of n=3 RMPs on L-H transition

On MAST the application of n=3 RMPs before the L-H transition can either suppress the L-H transition entirely or significantly delay it. Figure 9 shows an example from a shot with I_p=900 kA (shot 24560) which with 1.8 MW of beam power and without the application of RMPs goes into a type III ELMy H-mode at 0.27 s. If all the plasma parameters are kept constant and an n=3 RMP is applied in an odd parity configuration with 5.6 kAt before the time of the L-H transition, as in shot 24562, the H-mode transition is completely suppressed. To restore the H-mode the beam power has to be increased by ~33 % i.e. to 2.4 MW and in this case (not shown) the H-mode transition is delayed by ~80 ms. In order to produce an L-H transition at the same time as in the shot without the RMPs the beam power has to be raised to 3.3 MW (i.e. an increase of ~ 80%) as in shot 24564.

An analysis of the differences between the shots with and without RMPs shows that the density and temperature profiles are similar in both shots before the transition. One difference that has been observed is in the Lorentz component ($\vec{v}\times\vec{B}$) of the radial electric

field ($E_r^{v\times B}$), which has been measured using active Doppler spectroscopy of He^+ at the low field side mid-plane with a radial spatial resolution of 1.5 mm and a temporal resolution of 5ms. Figure 10 shows that in shot 24560 (without RMPs) the $E_r^{v\times B}$ remains approximately constant up until the time of the L-H transition. In shot 24562 (with RMPs), the $E_r^{v\times B}$ is identical initially but as the RMPs are applied the $E_r^{v\times B}$ increases (becomes more positive) by ~ 2 kVm^{-1} and remains high at the time that shot 24560 transitions into H-mode. If the RMP applied was off resonance (i.e. in this case an odd parity configuration was used) or the coil current was at or below a threshold value (4.8 kAt for this discharge) then there was no change in the radial electric field or in the H-mode access.

In all the H-mode discharges investigated, it is found that the L-H transition threshold power is increased if an n=3 RMP with sufficient strength is applied before the L-H transition and in all these shots at least a 30 – 40 % increase in beam power is required to re-establish the transition. A clear threshold coil current is observed; for example, in the case shown in Figure 9 a perturbation of 5.2 kAt suppresses the L-H transition at 1.8 MW whereas a perturbation of 4.8 kAt does not effect the transition at all. In order to try to determine which RMP related parameters may affect whether or not the L-H transition is suppressed, vacuum modelling has been performed on the shots for which the threshold coil current has been measured. Figure 11 shows the profiles of b^r_{res} and $\sigma_{Chirikov}$ obtained from vacuum modelling for shot 23409 (a lower SND discharge with I_p= 600 kA, q_{95}=3.2), shot 24459 (a CDN discharge with I_P=750 kA, q_{95}=5.2) , shot 24560 (a CDN discharge with I_P=900 kA, q_{95}=6.0) and shot 24878 (a SND discharge with I_P= 600 kA, q_{95}=10). The resonant field component (b^r_{res}) near to the plasma edge is similar in three of the four shots

(Figure 11a). There is a weak dependence of b^r_{res} on toroidal rotation velocity, with the shot with the smallest b^r_{res} (24878) having the smallest toroidal velocity. Due to the different magnetic shear the Chirikov profiles are different (Figure 11b) with a spread in $\Delta_{\psi Chirikov>1}$ which increases in proportion to q_{95} from 0.11 to 0.265 in ψ_{pol} space. Unfortunately E_r measurements before the L-H transition have only been made in the one discharge so it has not been possible to determine if the change in E_r is correlated with any of these parameters. For example, if a critical change in E_r were responsible it would be necessary to know how E_r changed with b^r_{res} in these shots in order to draw any conclusion.

4. Effect of n=3 RMPs on connected double null H-mode plasmas

In H-mode, for CDN plasmas just above the L-H transition threshold, the application of the RMPs is equivalent to a small decrease in input power. For example, the application of the RMPs can trigger more frequent ELMs in a type III ELMing discharge and can trigger type III ELMs in an ELM free discharge [4]. Initial experiments showed that the application of the RMPs to discharges with type I ELMs produced little effect on the ELM behaviour or pedestal characteristics. This was despite the fact that vacuum modelling using the ERGOS code showed that the stochastised layer (defined as the region for which the Chirikov parameter is greater than 1) had a radial extent wider than that correlated with ELM suppression in DIII-D **[10]**. However, there are many differences between the MAST and DIII-D discharges, including shape, aspect ratio and collisionality so if these parameters are important it may explain why ELM suppression was not achieved in these plasmas.

More recent experiments have shown that it is possible to increase the ELM frequency and decrease the ELM energy loss by carefully adjusting the q_{95} of the plasma. Figure 12 shows a series of shots where the q_{95} is lowered from 5.4 to 4.5, while an n=3 RMP was applied in odd parity (which is predicted to be more on resonance at lower q_{95})

with a current of 5.6 kAt in the coils from a time of 0.24 s. In the shot with q_{95} = 5.4 the RMPs have no effect, however, for the shot with q_{95} = 4.9 a drop in density is observed around 0.3 s and the ELM frequency thereafter increases. For the shot at q_{95}=4.5 a very rapid density pump out occurs at t=0.28 s leading to a back transition to L-mode before any impact on the ELM frequency can be established. In both cases the drop in density is associated with a burst of high frequency ELMs. The shots have also been repeated with no RMPs applied and in this case there was very little change in the ELM behaviour or H-mode duration with q_{95}. Similar, strong dependences of the observed effect of RMPs with q_{95} have been observed on DIII-D [11] and JET [12].

ERGOS modelling shows that as the q_{95} is lowered the magnetic perturbations become better aligned with the plasma q profile (Figure 13). Figure 14a shows how the normalised resonant component of the applied field (b^r_{res}) in the pedestal region increases from $5.5x10^{-4}$ for q_{95}=5.4 to $7x10^{-4}$ for q_{95}=4.9. However, the Chirikov profile remains about the same (see Figure 14b) and hence the width of the stochastic layer does not change (i.e. $\Delta_{\text{Chirikov}>1}$ = 0.21 in ψ_{pol}) because although the resonant field is increasing, the island overlap decreases due to the reduction in q_{95} and of the edge shear. This again indicates that the Chirikov parameter is not the main parameter in determining whether or not ELM mitigation is established.

MARS-F modelling has also been performed for these shots. The plasma surface displacement peaks at the outboard mid-plane at q_{95} = 5.4, where no effect is observed in the experiment. Whereas at q_{95} = 4.9, the computed surface displacement peaks near the X-points. A scan in q_{95} from 5.4 down to 4.5, shows a smooth transition from the mid-plane peaking to the X-point peaking. This can be seen in Figure 14c that shows a figure of merit defined as $F = |\zeta_n(\text{Xpt})/\zeta_n(\text{Mid})|$, which is the ratio of the peak value of the surface displacement (ζ_n) near the X-points to that at the mid-plane. The effect on the plasma is

observed for q95 ~ 4.9, which corresponds to F ~2.0. Of course the value of F is only relevant for finite sized perturbations; however, for ζ_n above a few mm, F seems more important than the absolute displacement.

The shot with q_{95}=4.9 has been repeated several times and the properties of the ELMs before and after the change in frequency established. Up until the sharp density pump out at 0.3 s the shots with and without RMPs have similar density, temperature and toroidal velocity profiles. Just after the density drop there is again little change in the velocity or temperature (ion or electron) profiles while the pedestal density decreases by ~30% (see Figure 15a). The pedestal characteristics before the density pump out move from those associated with type I ELMs on MAST to those previously found to be associated with type IV ELMs [13]. A similar effect has also been observed during Double Null discharges in DIII-D [14]. The net loss in pedestal pressure means that the stored energy reduces from 120 kJ to 106 kJ, while the ELM frequency (f_{ELM}) increases from ~ 100 to ~ 500 Hz and the energy loss per ELM (ΔW_{ELM}) decreases from a mean value of ~ 5kJ to ~ 1kJ i.e. consistent with $\Delta W_{ELM}.f_{ELM}$~ constant. However the peak power density at the target due to the ELM only decreases by a factor of ~2 due to the fact that the target power profile is narrower in the ELMs with lower energy.

The ELM coils reach full current at 0.24 s in this shot whereas the effect on the density only occurs at 0.29 s. During this period the toroidal rotation and q_{95} are approximately constant while the plasma stored energy and normalised beta increase slightly. The pedestal temperature increases and pedestal density decreases such that the pedestal collisionality (ν^*_e [15]) falls from ~1.5 at t=0.24 to ~0.5 at t=0.29 s (see Figure 16). Although it is not possible to say whether or not a particular value of ν^*_e is required in order for the RMPs to have an effect on the ELMs in MAST a minimum collisionality is required for ELM suppression in DIII-D [16]. However, this would suggest that a different

effect is happening in H-mode compared to L-mode where the pump out is observed at much higher collisionalities.

5. Effect of n=3 RMPs on single null divertor H-mode plasmas

To investigate if magnetic geometry can influence the effect of RMPs on ELM behaviour, SND discharges have been investigated. Due to the up-down symmetry in the divertor coils on MAST, SND discharges are usually produced by shifting the plasma downwards. In this lower SND magnetic configuration the plasma is far from the upper row of RMP coils and hence the perturbation is predominantly from the lower row of coils, which produces a much broader spectrum of magnetic perturbation. If the RMPs are applied with full current in both the upper and lower row of coils then a brief increase in the ELM frequency and decrease of the ELM size is observed, together with a decrease in the plasma density. Unfortunately this is then followed by a back transition to L-mode due to the fact that the RMPs cause a large braking to the toroidal plasma rotation, which is observed to extend all the way into the core of the plasma [4]. ERGOS calculations show that the maximum of the applied resonant field component can be shifted radially outwards by changing the ratio of the upper to lower currents (decreasing the lower coil current) and shifting the plasma vertically upwards by 2 cm. The magnetic perturbation spectrum for such a case where the coil current in the upper coils is 5.6 kAt while the current in the lower coils is 4.8 kAt is shown in Figure 17a. The peak in the perturbation is well aligned with the rational surfaces in the plasma leading to large values of the resonant field component (Figure 17b), which has a peak value of $b^r_{res} \sim 6.8 \times 10^{-4}$ near to the plasma edge. The Chirikov profile, Figure 17c, shows a broad region for which $\sigma_{Chirikov} > 1$, with $\Delta\sigma_{Chirikov>1} \sim 0.085$ in $\sqrt{\psi_{pol}}$ or 0.16 in ψ_{pol}. MARS-F calculations for this configuration show

that the plasma displacement is again peaked at the X-point with a figure of merit F = $|\zeta_n(\text{Xpt})/\zeta_n(\text{Mid})| = 1.5$.

The application of the RMPs in this configuration does reduce the braking substantially and has enabled the period with smaller ELMs to be maintained for up to 100 ms (see Figure 18). In this discharge the ELM frequency increases from 80 to 150 Hz, while the ELM energy loss decreases from 10 kJ to 6kJ. The pedestal density decreases from 3 to $2.5\text{x}10^{19}\text{m}^{-3}$ and the pedestal temperature remains unaltered at 300 eV which results in a 15 % decrease in stored energy. Unlike in the CDN case discussed in the last section, in the LSND plasmas the effect is very prompt after the application of the RMPs. This may be due to the fact that the edge collisionality is already quite low and ~ constant in this period with $\nu^*_e \sim 0.5$ at the pedestal top.

6. Summary and discussion

Experiments have been performed on MAST using internal (n=3) resonant magnetic perturbation coils. The application of the RMPs to L-mode discharges has shown a clear density pump out when the pitch angle at the low field side of the plasmas is well aligned with the applied perturbation. In all the discharges studied, pump out is only observed when the region for which the Chirikov parameter (calculated in the vacuum approximation) is greater than 1 ($\Delta_{\text{Chirikov}>1}$) is greater than 0.165 in ψ_{pol} space. Although this may be a necessary criteria to ensure pump out it can not be the only criteria since a shot which matches this criteria with both even and odd parity configurations of the coils only has a density pump out in even parity. Considering only vacuum modelling, this even parity configuration has only marginally better alignment of field lines with the perturbation than the odd parity one, casting some doubt on the alignment as a sole determining factor. Whether a pump out occurs or not may still be correlated with the size

of b^r_{res}: a value of $b^r_{res} \sim 5x10^{-4}$ being the minimum required to obtain a density pump out. More detailed scans of pitch angle alignment are needed to determine if this is a sufficient explanation. Determining the exact value of a threshold b^r_{res} would also require a careful inclusion of all non-axisymmetric field components.

Including the effect of the plasma response and screening due to plasma rotation decreases the size of these resonant components by up to an order of magnitude. It also leads to a new feature that is not accounted for in the vacuum modelling and that is the 3-D displacement of the plasma edge due to the RMPs. A clear correlation is observed between the location of the maximum of this displacement and density pump out: the pump out only observed when the displacement is larger at the X-point than at the LFS mid-plane. This may be an alternative explanation of the pump-out arising only in the even configuration in the shot where the vacuum Chirikov parameter and b^r_{res} for the odd configuration are similar.

The size of the displacement is affected by the plasma rotation; however, even relatively low plasma rotations, associated with Ohmic L-mode plasmas, are sufficient to provide considerable screening and this screening then evolves very weakly with increasing plasma rotation. This is found to be in agreement with the observation that the size of the pump out is not affected by an increase in toroidal rotation of the plasma suggesting that any screening is already fully effective at the lower value.

In a range of discharge types it has been found that if the RMPs are applied before the L-H transition, with sufficient strength, they can suppress the L-H transition. An increase in the radial electric field is associated with the application of the RMPs and may indicate that an increase in power is required to overcome the effect of this increase in E_r. Vacuum modelling for the range of shots covered does not indicate a clear correlation between any parameter and the H-mode suppression. In order to cast more light on this it

may be necessary to determine how the change in radial electric field is correlated with, for example, b^r_{res} in each discharge. In order to re-establish the H-mode at the same time then the heating power has to be increased by ~ 80 %, if a delay in the L-H transition can be tolerated then the input power needs to be increased by ~ 30 %. This may not be a problem in future devices as the coils could be applied after the L-H transition as long as the time from the L-H transition to the first ELM is longer than the current rise time in the RMP coils. However, it should be noted that when the RMPs are applied after the L-H transition to discharges in MAST that have an input power just above the L-H transition power (P_{LH}) then more frequent ELMs are triggered in a type III ELMing discharge and type III ELMs triggered in an ELM free discharge. Such a trend is consistent with decreasing the distance the plasma is above P_{LH}. This could have implications for future devices and needs to be explored as it may indicate an effective increase in P_{LH} occurs even if the coils are applied after the L-H transition.

In type I ELM-ing H-mode plasmas, which are a long way above P_{LH} (i.e. > $1.5xP_{LH}$), a similar alignment of the coils with similar perturbation strengths has no effect on the ELMs. This could be either due to the fact that the changes relative to P_{LH} are so small as not to be noticeable or because other screening effects, for example, diamagnetic rotation due to the better established pedestal become important.

However, in these type I ELM-ing plasmas an effect on the ELM frequency and size has been observed at particular q_{95} values, which is thought to be due to careful alignment of the magnetic perturbation with the plasma. In the best example seen to date the ELM frequency is increased by a factor of 5. The q_{95} scan shows that the effect is not correlated with the width of the region for which the Chirikov parameter is greater than 1 but again seems to be related in vacuum modelling to the size of the resonant field component in the pedestal region or in plasma response modelling to the location of the peak plasma displacement. The correlation of density pump out with the location of the peak plasma

displacement being near the X-point observed in the plasma response modelling may be related to the importance of the X-point in plasma fuelling and the particle balance that is required to maintain a constant plasma density.

Turning to other parameters that may be required in order to enable ELM mitigation/suppression, in both the CDN and SND discharges the effect on the ELMs is only observed when the edge collisionality $\nu^*_e \leq 0.5$. Since no density scan has been performed on these discharges it is not possible to say from the current data set if there is a collisionality threshold or not. However, on DIII-D ELM suppression is associated with a collisionality threshold $\nu^*_e < 0.32$ as well as to a range in normalised plasma pressure (β_N) with full suppression only being observed for $1.4 < \beta_N < 2.5$. It is not easy to see how such a β_N range should be scaled to another device, such as, a Spherical Tokamak which routinely operates at a higher value of β_N. The range in β_N could be related to, for example, some fraction of the no or ideal wall limit for a given Tokamak. For example, in one of the DIII-D discharges the n=1 no wall limit is ~ 2.1 and the ideal wall limit ~ 2.6 [17]. For the CDN MAST discharge considered here, the β limits have been calculated using the MISHKA-1 linear ideal MHD stability code [18]. The ideal no-wall limit for n=1 modes is found to be $\beta_N=4.25$ whereas the with-wall limit is $\beta_N=5.45$. Here the effective wall comprises the poloidal field coil casings as well as the distant vessel structure. Hence normalised to these values the MAST CDN and SND plasmas, which have $\beta_N \sim 4$ are in a similar operating space as the DIII-D plasmas.

However, these ideal kink calculations have been done for n=1, whereas it may be more appropriate if they were recomputed for the applied toroidal mode number of the applied RMP i.e. n=3. For the MAST case the wall-stabilised region narrows for higher

toroidal mode numbers, and for an ideal n=3 mode, with the same periodicity as the applied fields, the stability limits are $\beta_N^{no\text{-}wall}$=4.55 and β_N^{wall}=4.7 respectively. The experimental β_N~4 is 88 % of the n=3 no wall limit. It is interesting to note that a β_N scan performed using the MARS-F code shows that as the β_N no wall limit is approached a possible ideal kink mode response of the plasma may be triggered [7].

Finally, it has been suggested [19][20] that the RMPs are screened due to the rotation of the electron fluid and that RMPs can only penetrate at locations where the total electron velocity is zero. For the DIII-D plasmas where suppression is observed a narrow layer exists in the pedestal region where the sum of the $\vec{E}\times\vec{B}$ rotation of the plasma plus the electron diamagnetic rotation goes to zero [19]. To test if this criterion is approximately met in the MAST plasmas the $\vec{E}\times\vec{B}$ velocity and the electron diamagnetic velocity have been estimated for the CDN discharge with q95= 4.9 (shown in Figure 12) for which ELM mitigation is observed. Although there are uncertainties in these quantities, as can be seen from Figure 19, the total electron rotation velocity is consistent with having a zero inside the plasma near to the pedestal region ($V_{ExB}+V^*_e$ crosses zero at ψ_{pol} ~ 0.94), which is close to one of the resonant surfaces and hence with there being the possibility for RMP penetration. Future experiments on MAST will try to address some of these issues. The field penetration is most likely a non-linear process, with a threshold field being required initially to exert sufficient braking torque in order to allow the field to penetrate. This may explain why optimising the alignment of the RMPs with the plasma and hence optimising the size of the resonant components, appear to be correlated with the pump out in L-mode and also ELM mitigation in H-mode.

Acknowledgement

This work, part-funded by the European Communities under the contract of Association between EURATOM and CCFE, was carried out within the framework of the European Fusion Development Agreement. The views and opinions expressed herein do not necessarily reflect those of the European Commission. This work was also part-funded by the RCUK Energy Programme under grant EP/I501045.

References

[1] Loarte A *et al.*, 2003 *Plasma Phys. Control. Fusion* **45** 1594

[2] Evans T. *et al.*, 2004 *Phys. Rev. Lett*. **92** 235003

[3] Liang Y. *et al.*, 2007 *Phys. Rev. Lett.* **98** 265004

[4] Kirk A. *et al*., 2010 *Nucl. Fusion* **50** 034008

[5] Nardon E. *et al*., 2007 *J. Nucl. Mater.* **363-365** 1071

[6] Nardon E. 2007 "Edge Localized modes control by resonant magnetic perturbations" *PhD Thesis* Ecole Polytechnique

http://www.imprimerie.polytechnique.fr/Theses/Files/Nardon.pdf

[7] Liu Yueqiang *et al.*, 2010 *Phys. Plasmas* **17** 122502

[8] Liu Yueqiang *et al.*, "Modelling of Plasma Response to RMP Fields in MAST and ITER", Paper THS/P5-10, Proc. 23rd IAEA Fusion Energy Conference 2010, Daejeon Korea. Submitted to Nucl. Fusion.

[9] Liu Yueqiang, "Correlation between plasma response to resonant magnetic perturbation fields and density pump out", Submitted to Phys. Rev. Lett.

[10] Fenstermacher M.E. *et al.* 2008 Phys. of Plasma **15** 056122

[11] Schmitz O. *et al.*, 2010 *Phys. Rev. Lett*. **103** 165005

[12] Liang Y. *et al.*, 2010 *Phys. Rev. Lett*. **105** 065001

[13] Kirk A. *et al*., 2009 *Plasma Phys. Control. Fusion* **51** 065016

[14] Hudson B. *et al*., 2010 *Nucl. Fusion* **50** 064005

[15] Sauter O, Angioni C and Lin-Liu Y R 1999 *Phys. Plasmas* **6** 2834

[16] Burrell K.H. et al 2005 *Plasma Phys. Control. Fusion* **47** B37–B52

[17] Lanctot M. *et al.*, "Measurement and modelling of three-dimensional equilibria in DIII-D" Submitted to Phys. Plasmas.

[18] Mikhailovskii, Huysmans, Sharapov, Kerner, 1997 *Plasma Phys Rep* **23** 844

[19] Nardon E. *et al*., 2010 *Nucl. Fusion* **50** 034002

[20] Heyn M. et al., 2008 *Nucl. Fusion* **48** 024005

7. Figures

Figure 1 Time traces of the line average density ($\bar{n}_e$) and coil current (I_{ELM}) for L-mode shots with plasma current of a) 400 kA and b) 900 kA using coils in odd and even parity mode.

Figure 2 a) Poloidal profiles of the discharges with I_P= 400 and 900 kA. Plots of the component of the magnetic perturbation (vacuum approximation) perpendicular to the equilibrium flux surfaces as a function of toroidal angle (ϕ) and the poloidal angle in a straight field line co-ordinate system (θ^*) on the q=6 flux surface for discharges with I_P = b) 400 and c) 900 kA. The solid lines show the equilibrium field lines at the q=6 surface.

Figure 3 Poloidal magnetic spectra calculated in the vacuum approximation for a) a shot with I_P=400 kA and an even parity configuration of the coils and b) a shot with I_P=900 kA and an odd parity configuration of the coils. Superimposed as circles and dashed line are the q=m/3 rational surfaces of the discharge equilibrium.

Figure 4 Calculations in the vacuum approximation of a) the normalised resonant component of the applied field (b^r_{res}) and b) the Chirikov parameter profile produced for shots with I_P = 400 (900) kA with 5.6 kAt in the ELM coils in an even (odd) parity configuration.

Figure 5 Time traces of a) coil current (I_{ELM}) and b) line average density ($\bar{n}_e$) for an L-mode shot with 750 kA plasma current using coils in odd and even parity mode. Calculated profiles of c) the Chirikov parameter and d) the normalised resonant component of the applied field (b^r_{res}) produced with 5.6 kAt in the ELM coils. The calculations have been done for the ELM coils only and including the intrinsic plus error field correction fields in the vacuum approximation and taking into account the plasma response.

Figure 6 The amplitude of the normal displacement of the plasma surface computed by MARS-F as a function of poloidal angle where the coils are in odd or even parity configurations for the shots with I_P= a) 750 b) 400 and c) 900 kA.

Figure 7 Comparison of the effect of application of the RMPs in an even parity configuration on an I_P=400 kA Ohmic (Ω) or NBI heated shot. a) Time traces of the line average density ($\bar{n}_e$) and coil current (I_{ELM}) and b) the radial profile of the toroidal rotation velocity at a time or 0.3 s.

Figure 8 Calculations performed using MARS-F taking into account the plasma response of a) the normalised resonant component of the applied field (b^r_{res}) and b) the Chirikov

parameter profile produced for shots with I_P = 400 kA with 5.6 kAt in the ELM coils in an even parity configuration which are either Ohmically (Ω) or NBI heated.

Figure 9 Time traces of a) coil current (I_{ELM}) b) line average density ($\bar{n}_e$), and D_α for c) shot 24560 without RMPs and with 1.8 MW NBI and for d) shot 24562 with RMPs and with 1.8 MW NBI and for e) shot 24564 with RMPs and with 3.3 MW NBI respectively.

Figure 10 Profiles of the Lorentz component ($\vec{v} \times \vec{B}$) of the radial electric field (E_r) as a function of normalised poloidal flux (ψ_{pol}) for three time periods within shots with and without RMPs.

Figure 11 Calculations performed in the vacuum approximation of a) the normalised resonant component of the applied field (b^r_{res}) and b) the Chirikov parameter profile produced for values of the coil current sufficient to suppress the L-H transition in a range of shots.

Figure 12 Time traces of a) line average density ($\bar{n}_e$), and coil current and b-d) D_α for a series of shots with q_{95} in the range 5.4 to 4.5.

Figure 13 Poloidal magnetic spectra calculated in the vacuum approximation for an odd parity configuration of the coils for shots with q_{95} = a) 5.4, b) 4.9 and c) 4.5. Superimposed as circles and dashed line are the q=m/3 rational surfaces of the discharge equilibrium.

Figure 14 Calculations in the vacuum approximation of a) the normalised resonant component of the applied field (b^r_{res}) and b) the Chirikov parameter profile produced for shots with q_{95} = 4.5, 4.9 and 5.4 with 5.6 kAt in the ELM coils in an odd parity configuration. c) The ratio of the amplitude of the normal displacement of the plasma surface at the X-point compared to the mid-plane computed by MARS-F as a function of q_{95}.

Figure 15 The radial profiles of electron density (n_e) and temperature (T_e) obtained at t=316ms for shots with and without RMPs.

Figure 16 The time evolution of the electron collisionality at the top of the pedestal (ν^*_e) for a set of repeat shots. The vertical grey shaded area represents the time that the pump out is observed in the shots with RMPs applied.

Figure 17 Calculations performed in the vacuum approximation for a lower SND shot of a) the poloidal magnetic spectra with superimposed as circles and dashed line the q=m/3 rational surfaces of the discharge equilibrium, b) the profile of the normalised resonant component of the applied field (b^r_{res}) and c) the Chirikov parameter profile.

Figure 18 Time traces of a) the coil current (I_{ELM}) b) line average density ($\bar{n}_e$), and c) D_α for a lower SND shot with and without RMPs.

Figure 19 Profiles of the $\vec{E} \times \vec{B}$ rotation of plasma (V_{ExB}), the electron diamagnetic rotation V^*_e and the total rotation of the electrons ($V_{ExB}+V^*_e$).

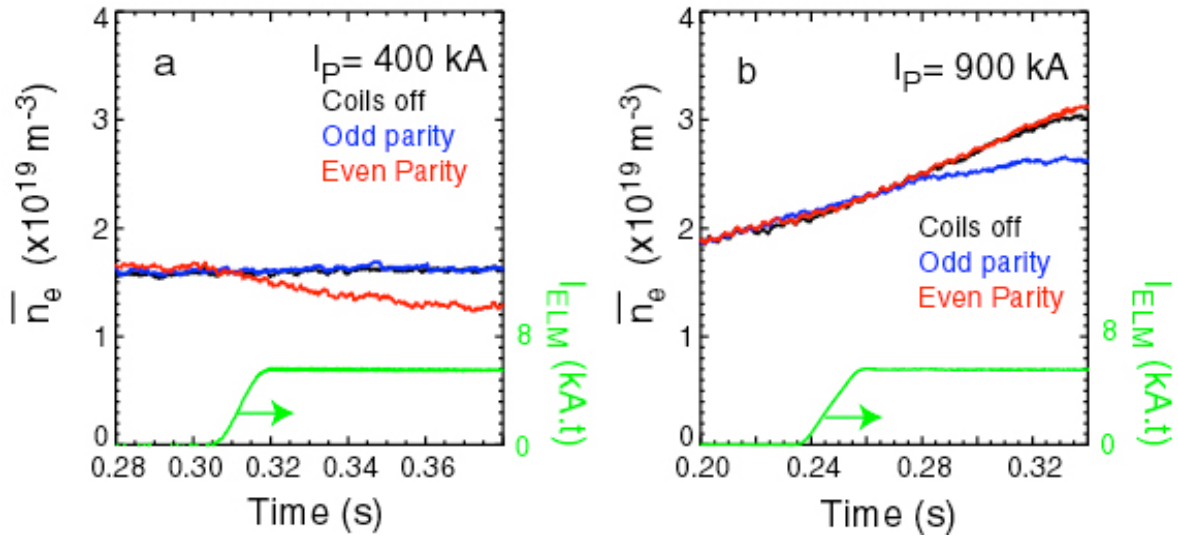

Figure 1 Time traces of the line average density ($\bar{n}_e$) and coil current (I_{ELM}) for L-mode shots with plasma current of a) 400 kA and b) 900 kA using coils in odd and even parity mode.

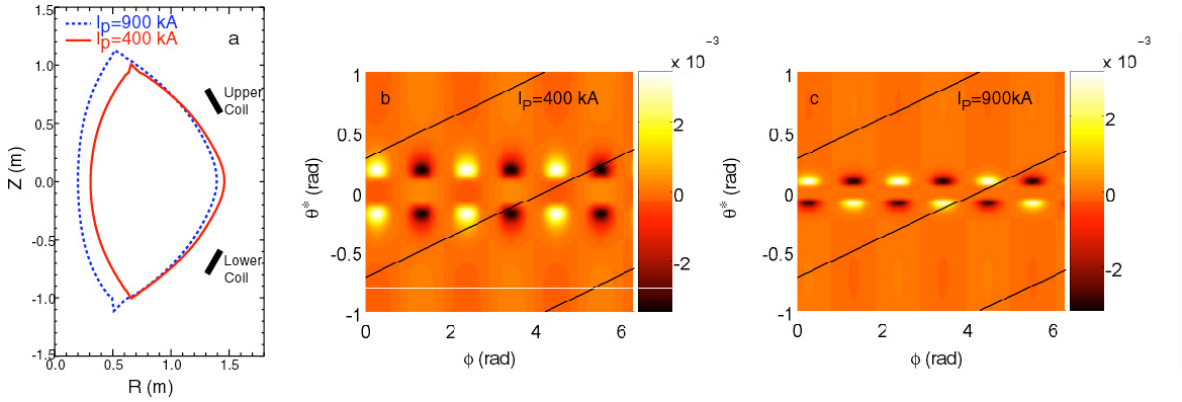

Figure 2 a) Poloidal profiles of the discharges with I_P= 400 and 900 kA. Plots of the component of the magnetic perturbation (vacuum approximation) perpendicular to the equilibrium flux surfaces as a function of toroidal angle (ϕ) and the poloidal angle in a straight field line co-ordinate system (θ*) on the q=6 flux surface for discharges with I_P = b) 400 and c) 900 kA. The solid lines show the equilibrium field lines at the q=6 surface.

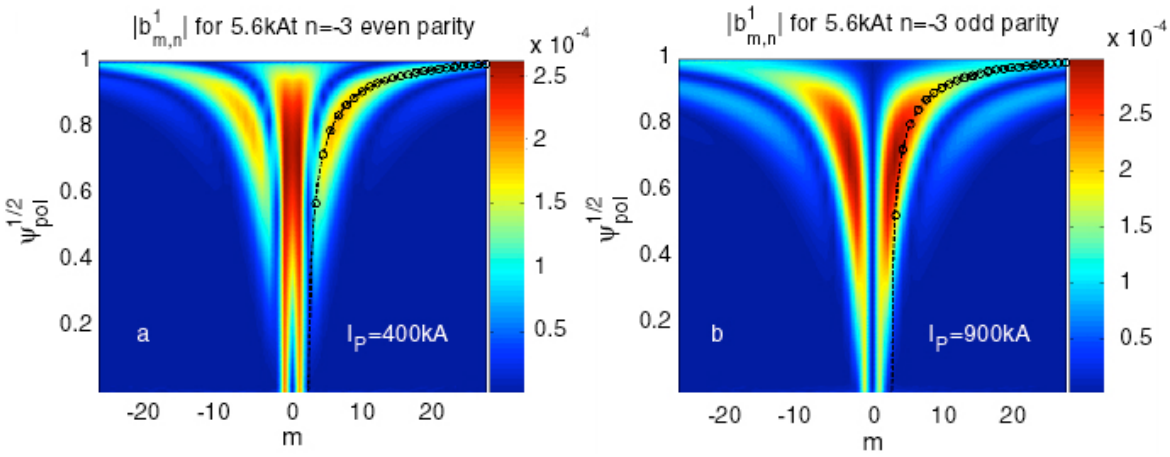

Figure 3 Poloidal magnetic spectra calculated in the vacuum approximation for a) a shot with I_P=400 kA and an even parity configuration of the coils and b) a shot with I_P=900 kA and an odd parity configuration of the coils. Superimposed as circles and dashed line are the q=m/3 rational surfaces of the discharge equilibrium.

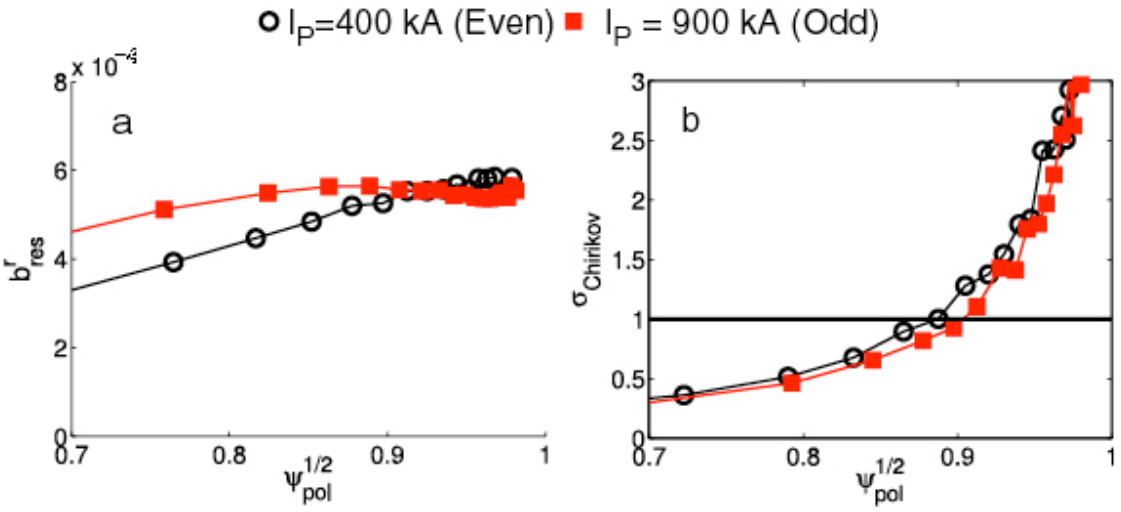

Figure 4 Calculations in the vacuum approximation of a) the normalised resonant component of the applied field (b^r_{res}) and b) the Chirikov parameter profile produced for shots with I_P = 400 (900) kA with 5.6 kAt in the ELM coils in an even (odd) parity configuration.

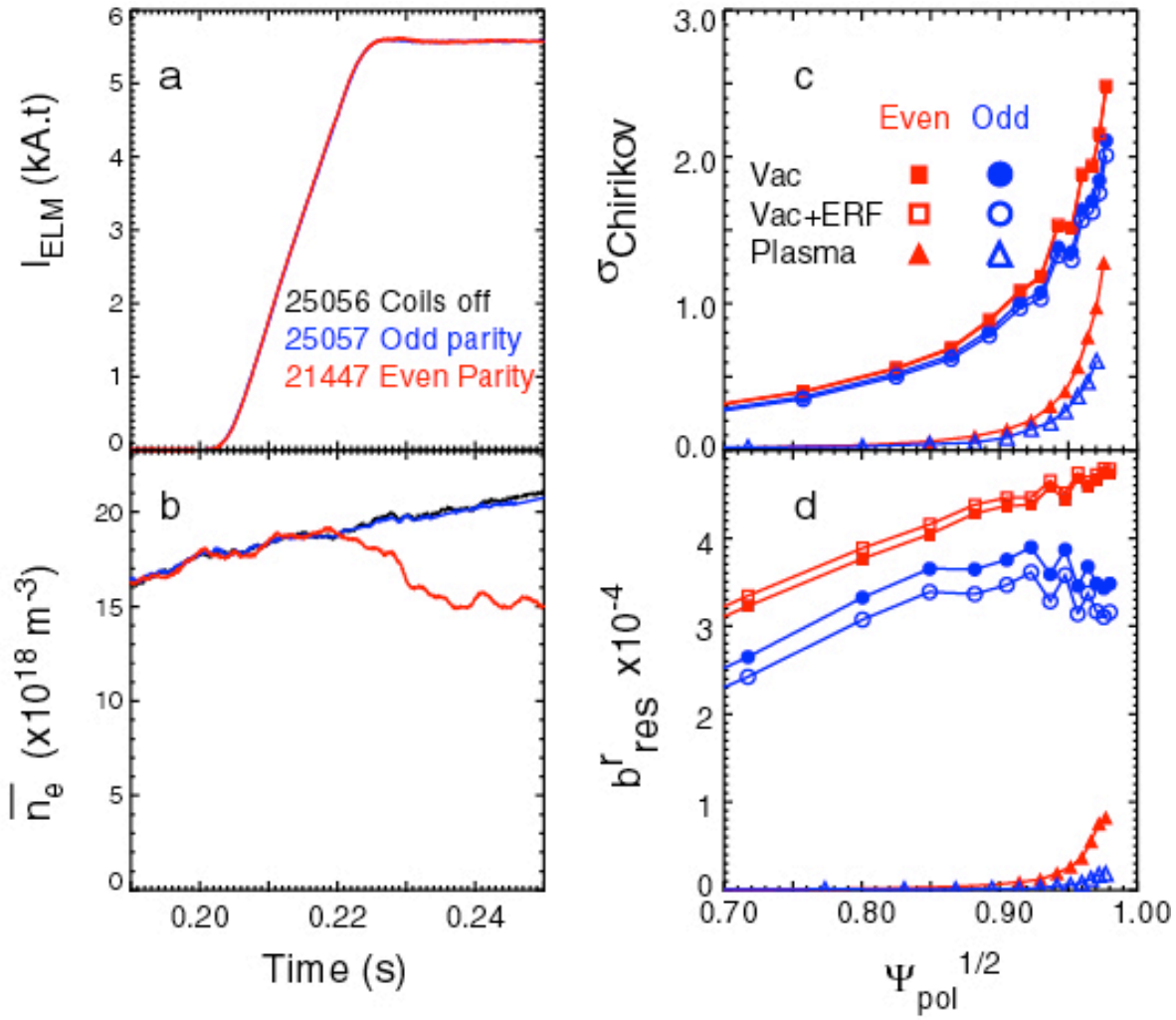

Figure 5 Time traces of a) coil current (I_{ELM}) and b) line average density ($\bar{n}_e$) for an L-mode shot with 750 kA plasma current using coils in odd and even parity mode. Calculated profiles of c) the Chirikov parameter and d) the normalised resonant component of the applied field (b^r_{res}) produced with 5.6 kAt in the ELM coils. The calculations have been done for the ELM coils only and including the intrinsic plus error field correction fields in the vacuum approximation and taking into account the plasma response.

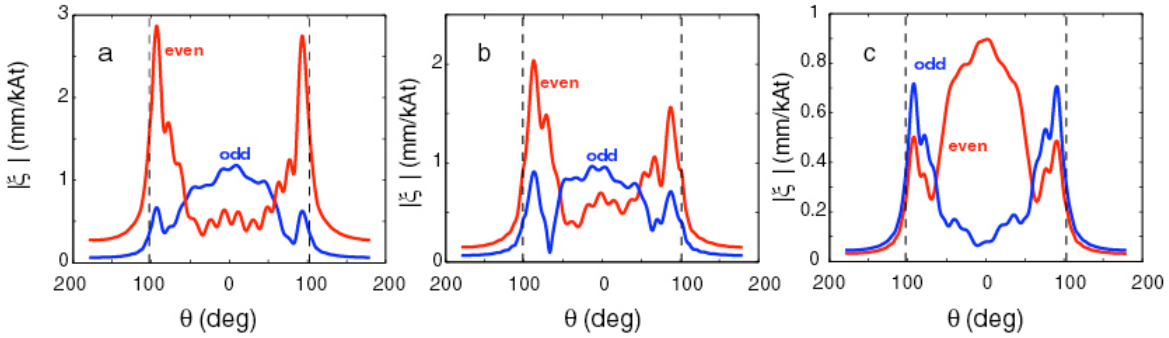

Figure 6 The amplitude of the normal displacement of the plasma surface computed by MARS-F as a function of poloidal angle where the coils are in odd or even parity configurations for the shots with I_P= a) 750 b) 400 and c) 900 kA.

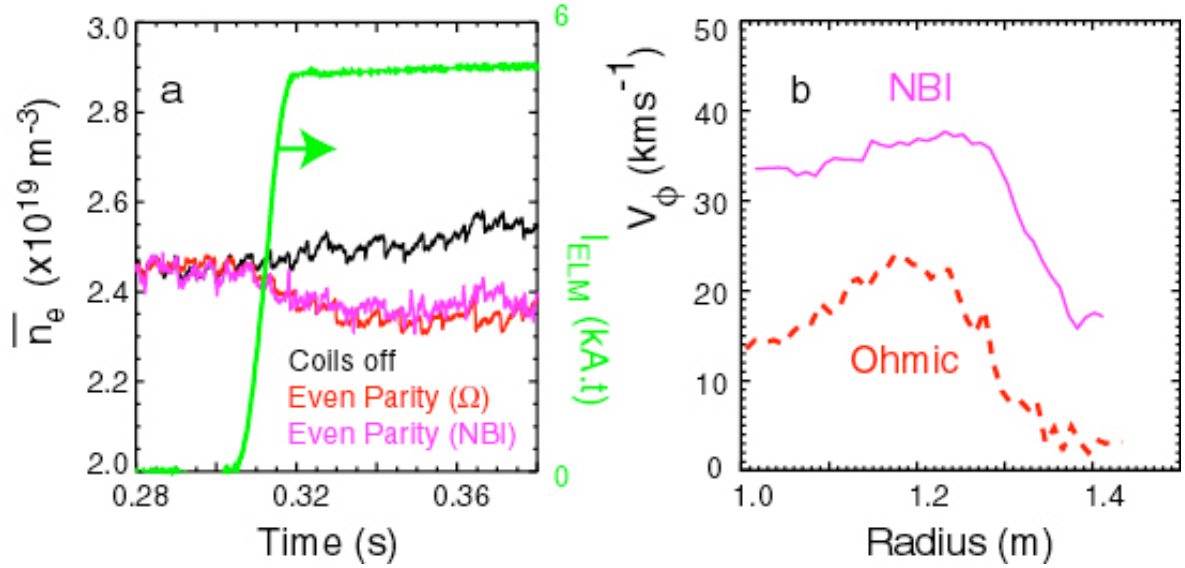

Figure 7 Comparison of the effect of application of the RMPs in an even parity configuration on an I_P=400 kA Ohmic (Ω) or NBI heated shot. a) Time traces of the line average density ($\bar{n}_e$) and coil current (I_{ELM}) and b) the radial profile of the toroidal rotation velocity at a time or 0.3 s.

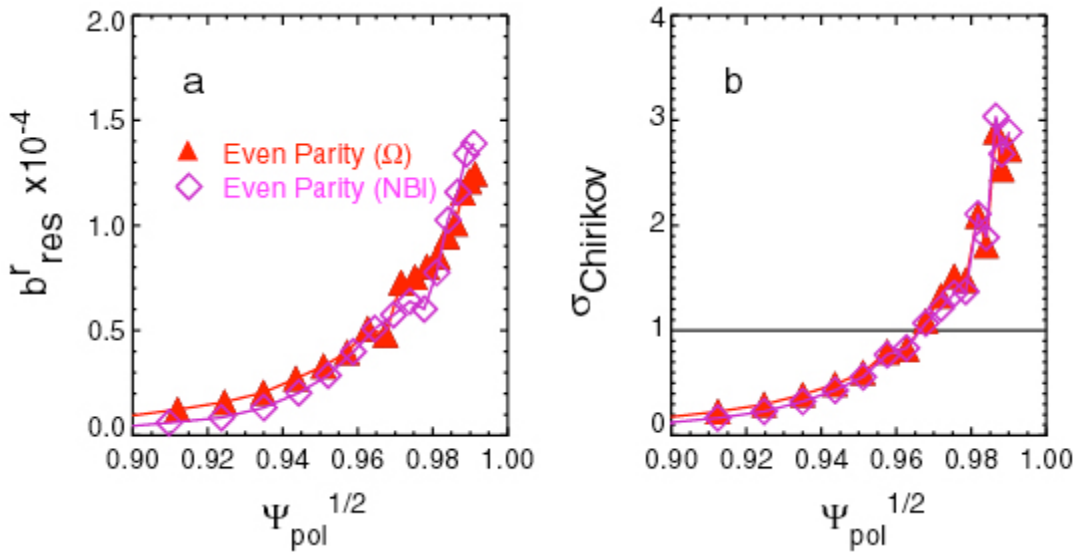

Figure 8 Calculations performed using MARS-F taking into account the plasma response of a) the normalised resonant component of the applied field (b^r_{res}) and b) the Chirikov parameter profile produced for shots with I_P = 400 kA with 5.6 kAt in the ELM coils in an even parity configuration which are either Ohmically (Ω) or NBI heated.

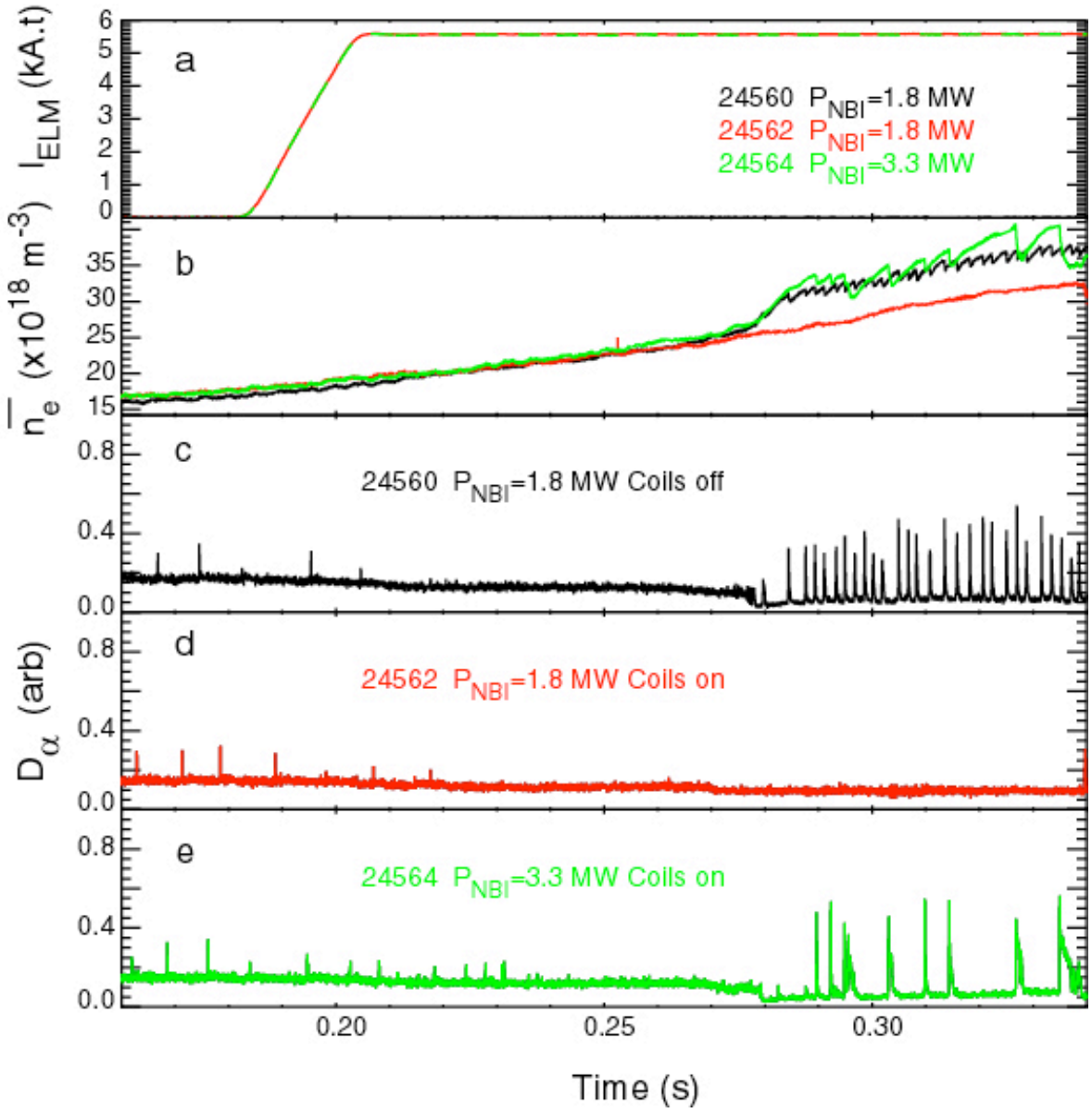

Figure 9 Time traces of a) coil current (I_{ELM}) b) line average density ($\bar{n}_e$), and D_α for c) shot 24560 without RMPs and with 1.8 MW NBI and for d) shot 24562 with RMPs and with 1.8 MW NBI and for e) shot 24564 with RMPs and with 3.3 MW NBI respectively.

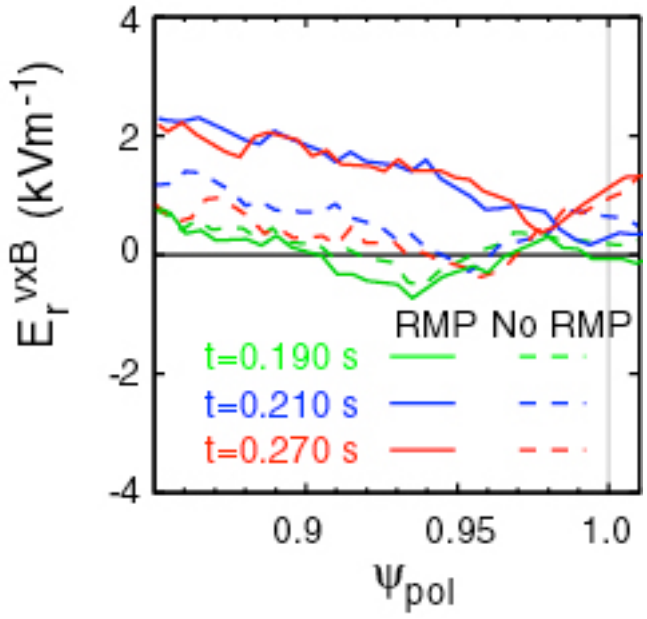

Figure 10 Profiles of the Lorentz component ($\vec{v} \times \vec{B}$) of the radial electric field (E_r) as a function of normalised poloidal flux (ψ_{pol}) for three time periods within shots with and without RMPs.

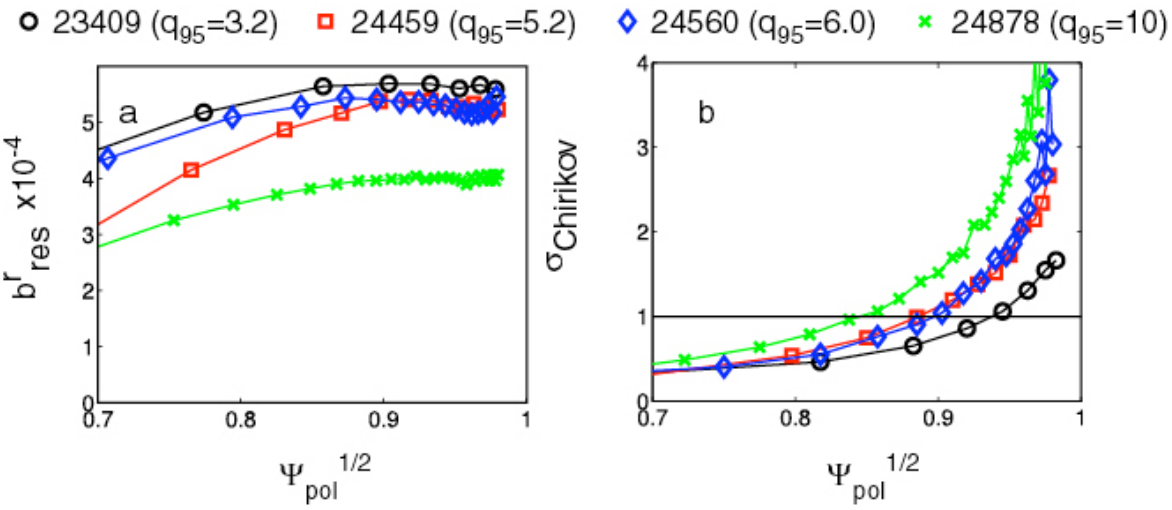

Figure 11 Calculations performed in the vacuum approximation of a) the normalised resonant component of the applied field (b^r_{res}) and b) the Chirikov parameter profile produced for values of the coil current sufficient to suppress the L-H transition in a range of shots.

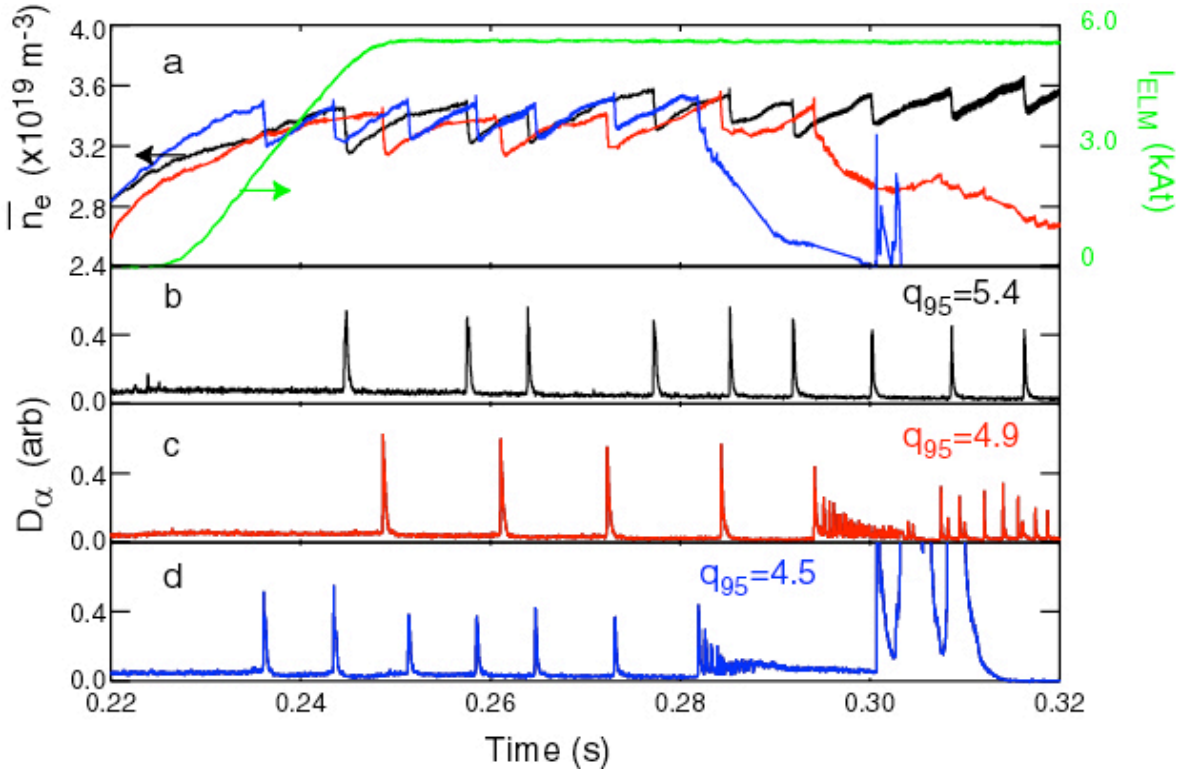

Figure 12 Time traces of a) line average density ($\bar{n}_e$), and coil current and b-d) D_α for a series of shots with q_{95} in the range 5.4 to 4.5.

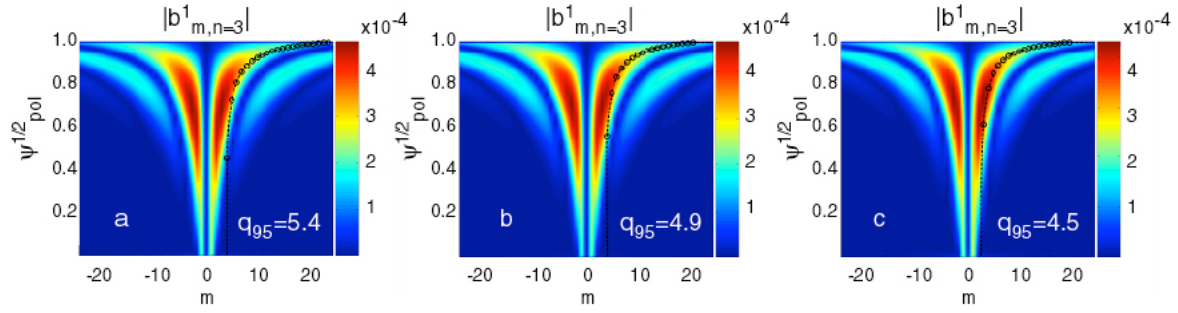

Figure 13 Poloidal magnetic spectra calculated in the vacuum approximation for an odd parity configuration of the coils for shots with q_{95} = a) 5.4, b) 4.9 and c) 4.5. Superimposed as circles and dashed line are the q=m/3 rational surfaces of the discharge equilibrium.

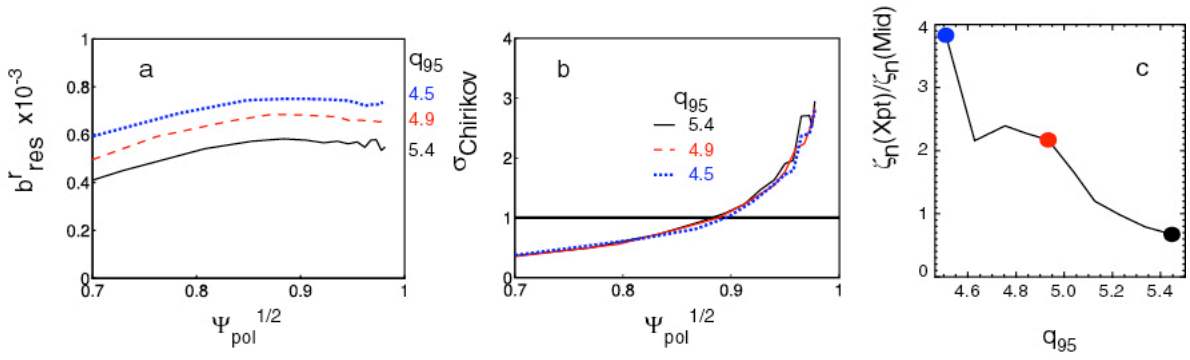

Figure 14 Calculations in the vacuum approximation of a) the normalised resonant component of the applied field (b^r_{res}) and b) the Chirikov parameter profile produced for shots with q_{95} = 4.5, 4.9 and 5.4 with 5.6 kAt in the ELM coils in an odd parity configuration. c) The ratio of the amplitude of the normal displacement of the plasma surface at the X-point compared to the mid-plane computed by MARS-F as a function of q_{95}.

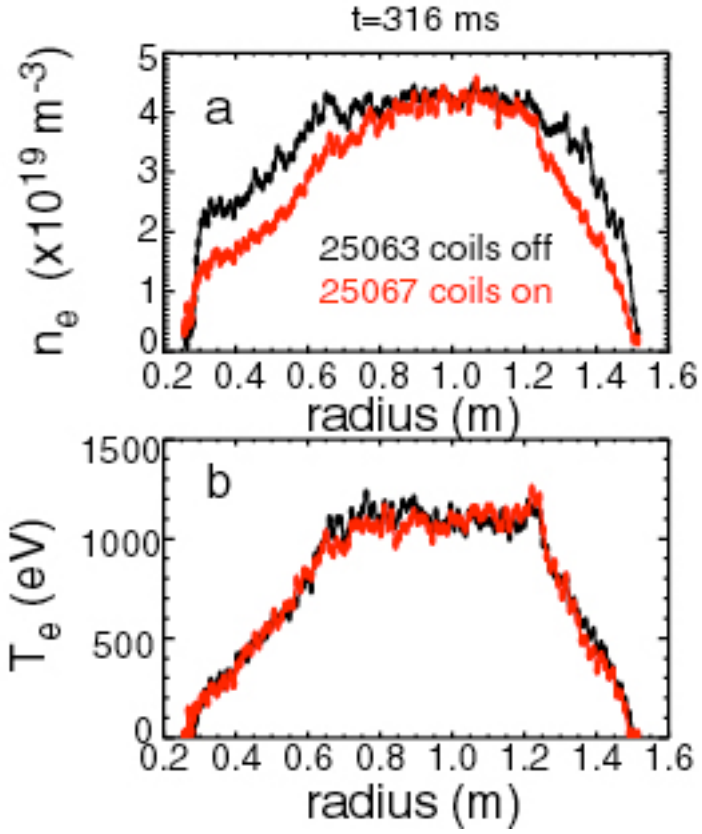

Figure 15 The radial profiles of electron density (n_e) and temperature (T_e) obtained at t=316ms for shots with and without RMPs.

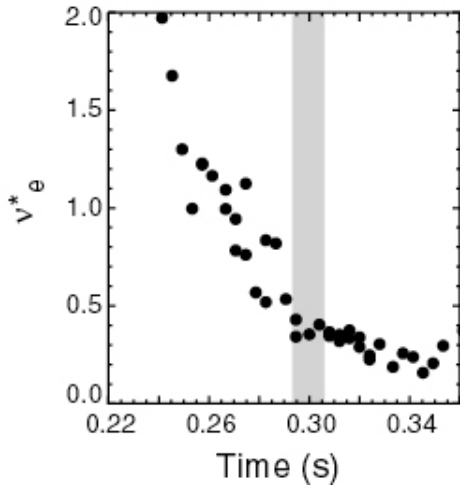

Figure 16 The time evolution of the electron collisionality at the top of the pedestal (ν^*_e) for a set of repeat shots. The vertical grey shaded area represents the time that the pump out is observed in the shots with RMPs applied.

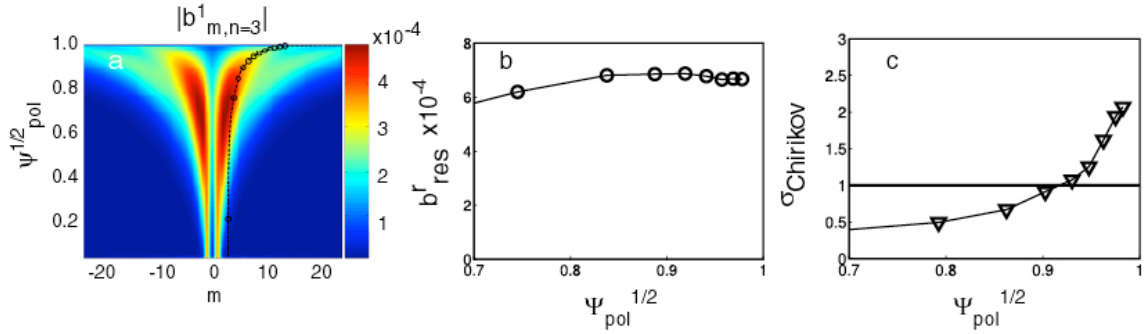

Figure 17 Calculations performed in the vacuum approximation for a lower SND shot of a) the poloidal magnetic spectra with superimposed as circles and dashed line the q=m/3 rational surfaces of the discharge equilibrium, b) the profile of the normalised resonant component of the applied field (b^r_{res}) and c) the Chirikov parameter profile.

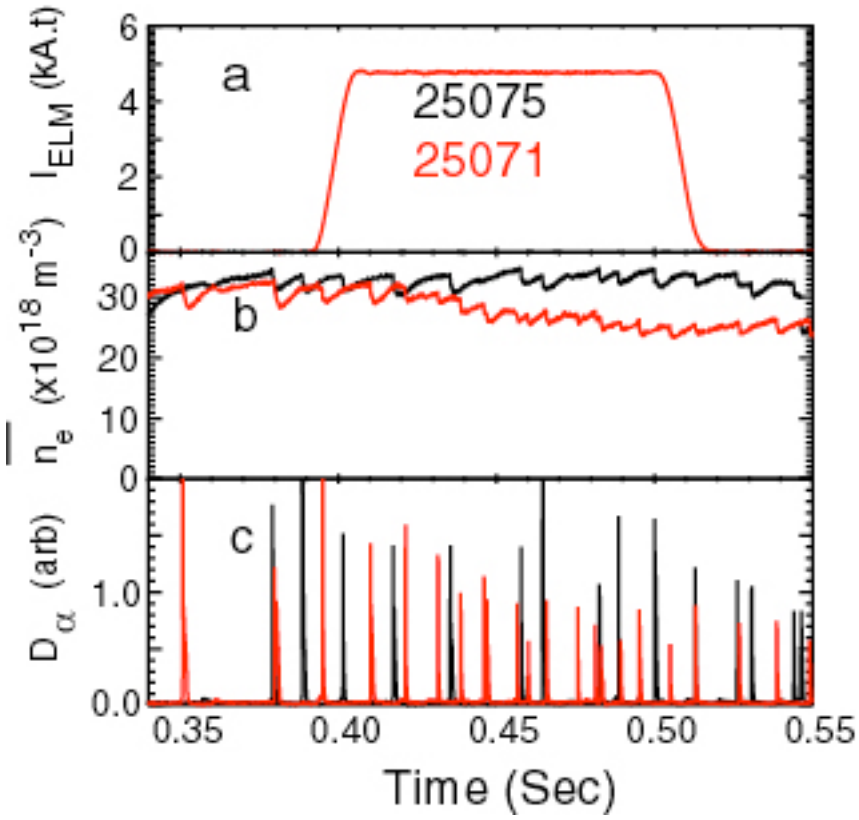

Figure 18 Time traces of a) the coil current (I_{ELM}) b) line average density ($\bar{n}_e$), and c) D_α for a lower SND shot with and without RMPs.

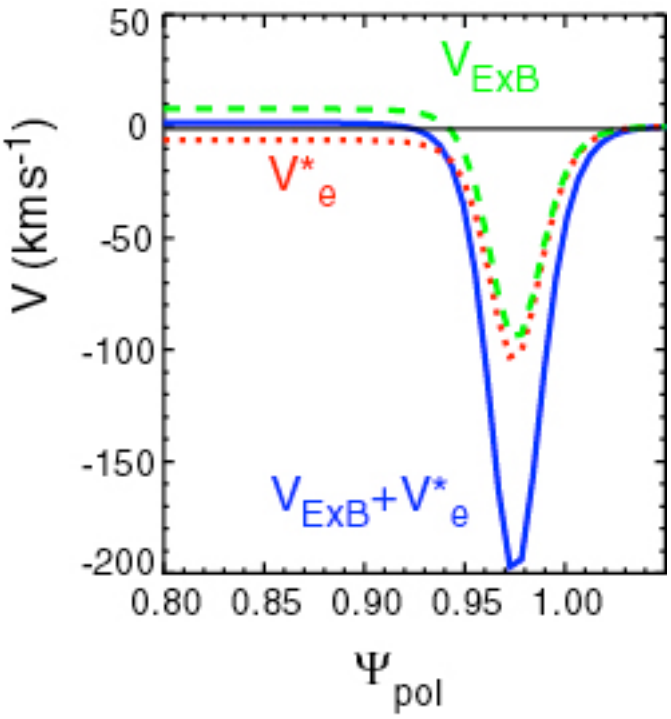

Figure 19 Profiles of the $\vec{E} \times \vec{B}$ rotation of plasma (V_{ExB}), the electron diamagnetic rotation V^*_e and the total rotation of the electrons ($V_{ExB}+V^*_e$).